PCCP

Topology induced Crossover between Langevin, Subdiffusion, and Brownian Diffusion Regimes in Supercooled Water

Journal:	*Physical Chemistry Chemical Physics*
Manuscript ID	CP-ART-10-2022-004645.R2
Article Type:	Paper
Date Submitted by the Author:	14-Mar-2023
Complete List of Authors:	Zhu, Kaicheng; Hong Kong University of Science and Technology Naserifar, Saber; University of Southern California, Chemical Engineering; California Institute of Technology Goddard III, William; California Institute of Technology Su, Haibin; The Hong Kong University of Science and Technology, Department of Chemistry

Topology induced Crossover between Langevin, Subdiffusion, and Brownian Diffusion Regimes in Supercooled Water

Kaicheng Zhu[1], Saber Naserifar[2], William A. Goddard III[2,*], and Haibin Su[1,*]
[1]*Department of Chemistry, The Hong Kong University of Science and Technology, Kowloon, Hong Kong*
[2]*Materials and Process Simulation Center, California Institute of Technology, Pasadena, California, USA 91125*

**To whom correspondence should be addressed. Email: wag@caltech.edu; haibinsu@ust.hk*

Despite extensive studies of supercooled water, it remains challenging to understand its peculiar dynamic anomalous properties. In this work, we integrated full atomistic simulations of supercooled water over the temperature range of room temperature to 200 K using quantum-mechanics-based polarizable force field with the dressed dynamics method that coupled fast collision events and slow reorganization dynamics of the hydrogen-bond networks. Our analysis unveils the salient multiscale features in transient relaxation dynamics of supercooled water. For instance, classical Langevin behavior dominates at fast timescales, while long-time relaxations unveil two different activation barriers in two temperature regions: below and above 230 K. The modulation of entropy spectrum by temperature is elucidated in terms of a three-state model underlined by the complexity of the water dynamics associated with a topological transition of strong hydrogen-bond network. This state-dependent network topology is quantitatively characterized by power-law exponents of inverse network connectivity from 200 to 298 K. The work provides valuable guidance for further studies on the transient relaxation dynamics of supercooled water.

Keywords: supercooled water, transient relaxation dynamics, hydrogen-bond network, topological transition, inverse connectivity

I. INTRODUCTION

Water is famously different from an ideal simple liquid, showing anomalous properties at temperatures near and below standard ambient conditions, especially in the supercooled state[1–5]. These anomalies of supercooled water are manifested by various properties that depend on the changes in the fluid structure[6–8]. The self-diffusion in the liquid state is associated with relaxation of the microscopic structure, as quantitatively described by the Stokes-Einstein relation. However, the breakdown of Stokes-Einstein relation from room temperature to the deeply supercooled region, a key anomalous phenomena in liquid water, has been reported over decades, but the underlying physics based mechanism remains unclear[9–12]. Another puzzle is the anomalous transport property of supercooled water at the fragile-to-strong transition. The fragile-to-strong transition characterizes the change from a non-Arrhenius to an Arrhenius temperature dependence of viscosity and diffusion coefficient at the glass transition[13]. But in supercooled water, this transition is observed at around 230 K, much higher than the glass-transition temperature[14]. Recently, Xu et al.[15] used a pulsed-laser-heating technique to measure the crystalline-ice growth rate for the temperature range of 126 to 262 K from which they extracted the liquid-water diffusivity and also identified the fragile-to-strong transition at 230 K. Researchers have made substantial efforts to explain this phenomenon from various perspectives. For instance, statistical analysis based on a two-state model attributed this transition as a crossover of two separate Arrhenius relations of the long-term diffusion coefficient[16]. Furthermore, a 1D-to-2D topological transition of the strong hydrogen-bond (HB) network has been discovered around 230 K, that provides microscopic insight into the dramatic decrease of the diffusivity and the fragile-to-strong transition in supercooled water[17,18]. However, the transient relaxation dynamics of water structure remains obscure.

One recent theoretical development of the dressed diffusion model greatly improved the understanding of the anomalous diffusive motion in a wide range of physical, chemical and biological systems[19,20]. The fundamental idea of the dressed diffusion is to generalize the classical diffusion theory of Langevin dynamics with a dynamic dressing field that characterizes inhomogeneity in the system. The coupling between the spatial motion of the particles and the transient relaxation dynamics of this effective field elucidates various anomalous diffusion behavior at different spatio-temporal scales, which sheds light on the diffusion anomaly in supercooled water. In addition, the molecular dynamics (MD) studies have been advanced with the RexPoN force field (FF)[21] for which all components, including bond breaking (Rex), polarization (Po), and van der Waals (vdW) non-bonded (N) energy terms are based entirely on quantum mechanics with no empirical input. In comparison with other empirical FFs[22,23], RexPoN is the first FF to quantitatively reproduce the experimental first peak in the O-O radial distribution function[17,24]. Thus RexPoN holds great promise to explain the detailed

dynamics of HB network in supercooled water structures[17,18].

In this work, we use the MD simulations with RexPoN FF and the dressed diffusion model to explain the time-resolved relaxation dynamics underlying the anomalous diffusion property in supercooled water: this explicitly shows the coupled two-scale relaxation dynamics:

- the fast relaxation process of barrierless collisional interaction and
- the slow relaxation process of reorganization of HB network.

Based on MD simulations with the RexPoN FF, we show that the anomalous behavior of the translational diffusion in supercooled water is manifested through the evolution of mean square displacement (MSD) over 6 orders of magnitude in time from femto- to nano-second. The fast relaxation dynamics follows a mechanism similar to classical Langevin dynamics, while the slow relaxation dynamics exhibits a notably strong temperature dependence. These slow dynamics lead to two distinct Arrhenius relations at separate temperature regions with a transition temperature at 228±3 K, in good agreement with both the measured fragile-to-strong transition and the 1D-2D topological transition of strong HB network at around 230 K. We extract the activation enthalpy and entropy for both temperature regions, finding a three-state model that provides a unified account for the physico-chemical dynamics of HB network from 298 K to 200 K. This model further correlates the different states with distinct HB-network motifs to explain the pivotal role of the underlying topological connectivity of strong HB network in the activation processes, leading to translational dynamic motions. In addition, inspired by the inverse participation ratio analysis[25–27] and persistent homology[28,29], we use the Laplacian-matrix-derived inverse connectivity to conduct a direct quantification of the temperature effect on the topological order of strong HB network.

II. MODEL, RESULTS AND DISCUSION

A. Coupling Fast and Slow Dynamics

A dressed dynamics model has been recently developed to study the anomalous diffusive motion in the liquid system far from homogeneous equilibrium[19]. This model generalizes classical Langevin dynamics with the spatio-temporal coupling between the probed particle and the environmental medium[20]. The tracked molecule is modeled as an ideal particle with no explicit internal degree of freedom, e.g., polarization, so its kinetic state is described by instantaneous spatial velocity $\boldsymbol{v}(t)$. The state of the surrounding liquid medium is modeled as a coupling field $\boldsymbol{\phi}(x,t)$ with explicit space-time dependence to characterize the nature of the many-particle system with bonding interactions that build the non-local spatial correlation, as illustrated in Fig. 1(a). Thus, the coupled particle-medium dynamics is formulated as follows:

$$\begin{bmatrix} \frac{d\boldsymbol{v}}{dt} \\ \frac{\partial \boldsymbol{\phi}}{\partial t} \end{bmatrix} = -\begin{bmatrix} \gamma_v & 0 \\ 0 & \hat{\gamma}_\phi \end{bmatrix}\begin{bmatrix} \boldsymbol{v} \\ \boldsymbol{\phi} \end{bmatrix} + \begin{bmatrix} \boldsymbol{R_v} \\ \boldsymbol{R_\phi} \end{bmatrix} + \hat{F}\begin{bmatrix} \boldsymbol{v} \\ \boldsymbol{\phi} \end{bmatrix} \quad (1)$$

where γ_v is the dissipative rate of the self-relaxation caused by friction or damping of the target particle and $\boldsymbol{R_v}$ is the associated fluctuation force. The operator $\hat{\gamma}_\phi$ describes the intrinsic dynamic dissipation of the medium, and similarly, $\boldsymbol{R_\phi}$ is the fluctuation force of the liquid environment. $\hat{F}$ is the coupling operator that gives the cross interaction between the particle and the medium. In the linear-response region, Eq. (1) can be written in a reduced form as follows:

$$\frac{d}{dt}\begin{bmatrix} v \\ \phi \end{bmatrix} = -\begin{bmatrix} \gamma_v & N \\ -M & \gamma_\phi \end{bmatrix}\begin{bmatrix} v \\ \phi \end{bmatrix} + \begin{bmatrix} R_v \\ R_\phi \end{bmatrix} \quad (2)$$

where M and N are two cross-coupling parameters quantifying the particle-medium interactions in a linear fashion, and γ_ϕ is the mean self-relaxation rate of the surrounding medium. In this simple formalism, the space-correlated cross coupling described by $\hat{F}$ is integrated into M and N in an implicit manner, so these two parameters characterize the net effect of both local and non-local interactions between the particle and medium. The stochastic motion of the tracked particle is thus coupled to the fluctuation-dissipation dynamics of the simplified dressing field ϕ through an exponential-decay memory kernel[19]. Eq. (2) has an exact analytical solution in the close form, which yields the MSD of the particle as:

$$\mathrm{MSD} = 2\langle v^2\rangle\left[b_1\left(\frac{t}{a_1} - \frac{1-e^{-a_1 t}}{a_1^2}\right) + b_2\left(\frac{t}{a_2} - \frac{1-e^{-a_2 t}}{a_2^2}\right)\right] \quad (3)$$

where $\langle v^2\rangle$ is the ensemble average of the square velocity, $a_{1,2} = \frac{1}{2}\left[\gamma_v + \gamma_\phi \pm \sqrt{(\gamma_v - \gamma_\phi)^2 - 4MN}\right]$ are the dressed relaxation rates associated with different timescales and $b_i = \frac{a_i - \gamma_\phi}{a_i - a_{3-i}}$ are the associated amplitudes for each mode. The general feature of time-dependent MSD of dressed diffusion is shown in Fig. 1(b) and compared with classical Langevin dynamics that explains the relaxation process from ballistic motion to Brownian diffusion. In dressed diffusion, the two-scale relaxation mechanism leads to the continuous crossover among three distinct dynamic regimes: a fast relaxation process with the same scaling behavior of Langevin dynamics, an intermediate sub-diffusion regime where the spatial motion is temporarily confined, and an asymptotic long-time limit of Brownian diffusion where MSD increases linear with time. This general feature is widely observed in a diverse range of liquid and complex soft-matter systems[9,12,19,30]. From the MSD curve, it is clearly

shown that the theory of dressed diffusion is a minimal model for this continuous crossover, because it involves only four elementary parameters: $\langle v^2 \rangle$, γ_v, γ_ϕ, and MN. Although M and N are clearly defined as two separate coupling parameters in Eq. (2), the effective coupling strength affecting the MSD behavior is their product MN, instead of their respective values, as shown in Eq. (3). Importantly, the dressed diffusion model provides the explicit account for the diffusion coefficient using these four parameters:

$$D_{DD} = \frac{\langle v^2 \rangle \gamma_\phi}{\gamma_v \gamma_\phi + MN} \quad (4)$$

This description is better than the classical Stokes-Einstein relation where the diffusion coefficient is expressed with a single relaxation timescale. This improvement is helpful to provide the insight into the breakdown of the Stokes-Einstein relation in supercooled water, which will be further discussed in the following section.

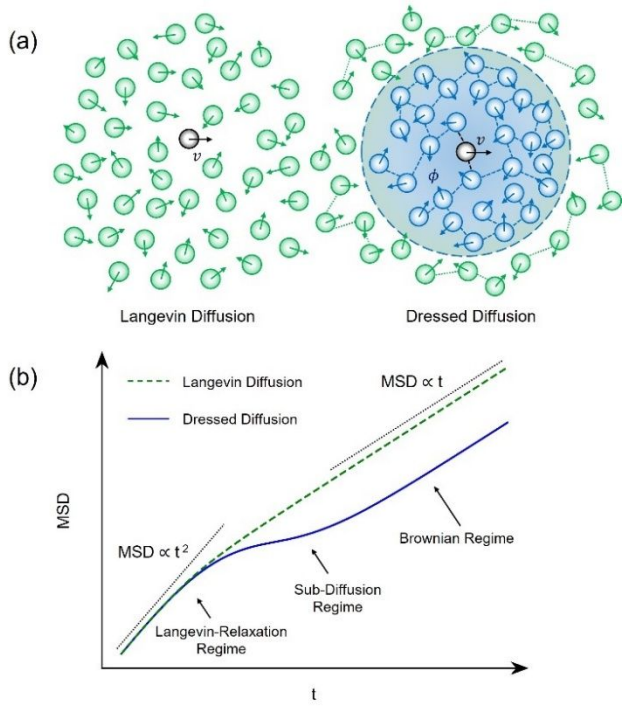

Figure 1. (a) Schematic comparison between Langevin diffusion and dressed diffusion. The velocity of every particle is denoted by the attached arrow. The target particle is labeled in black. The bonding interaction between particles is denoted by dotted lines. The coupling field ϕ is highlighted as the blue-shaded region. (b) The log-scale time-dependent MSD in dressed diffusion and Langevin diffusion. The dressed diffusion is shown by the blue solid line, and Langevin diffusion is shown by the green dashed line.

B. Dressed Diffusion Behavior in Supercooled Water

In supercooled water, the HB network at low temperature induces microscopic inhomogeneity with complex structural orders in the deeply cooled water[18]. The dynamic reorganization of the HB network strongly depends on temperature. The spatial translational motions of water molecules reflect delicate interactions among them in the non-innocent HB network. The dressed diffusion model[19,20], as an extension of Langevin equation, is capable of taking into account the coupling between individual water molecules and HB network in the form of dressed interaction as illustrated in Fig. 1(a). In liquid water, the translational self-diffusion is measured by single-particle tracking, while the stochastic spatial motion of water molecules is described by the generalized Langevin dynamics based on the dressed diffusion model [Eq. (2)]. The translational dynamics is characterized by the continuous evolution of the velocity v of the target water molecule, while the time-dependent dressing field ϕ quantifies the dynamic heterogeneity involving the collective non-bonded and HB interactions from the surrounding water molecules in a dynamical mean-field manner.

We conducted MD simulations with RexPoN FF of flexible water model at various temperatures. All supercooled simulations were carried out in the *NVT*-MD ensemble along the 1 atm density line. The experimental densities were used for temperatures above 240 K, while for temperatures below 240 K, we used the extrapolation of Kim *et al*[31]. To compute the MSD data, we ran the *NVT*-MD simulations with flexible water model after thermal equilibration (See Supporting Information).

In Fig. 2(a), the MSD of dressed diffusion model [Eq. (3)] is fitted to the trajectories from the MD simulation with RexPoN FF. With the explicit multiscale formalism in a simple analytical close form, the dressed diffusion accurately reproduces the time-dependent MSD of water molecules with the overall relative deviation less than 1% across all the timescales from femto- to nano-second for the broad temperature window from above room temperature to the deeply supercooled region at 200 K. This quantitative consistency elucidates the mechanism of the dynamic crossover between three distinct regimes: Langevin-relaxation, sub-diffusion, and Brownian diffusion. Within 100 fs, the time-dependent evolution of MSDs shows a continuous shift from a quadratic relation (MSD $\propto t^2$) toward a linear relation (MSD $\propto t$). This process is explained by Langevin equation describing the continuous particle motion with both frictional force and random force. In classical Langevin dynamics, the instantaneous velocity of the particle loses autocorrelation due to stochastic fluctuation-dissipation interactions, resulting in a transition of the particle's spatial kinetics from ballistic motion towards Brownian motion[32,33]. In the intermediate sub-diffusion regime, ranging from several pico-seconds to around nano-second as temperature drops, the increase of MSD is strongly hindered as the water molecules are locally confined in the polymeric cages formed by HB network. At

timescales beyond the HB lifetime, the HB network dynamically reorganizes through breaking and rebuilding of the HBs, leading to alterations in the caging structure that allows delocalization of the water molecules. Since the velocity autocorrelation has mostly decayed at the fast timescale before the cages diminish, this relaxation process at the slow timescale results in the long-time crossover from sub-diffusion to Brownian regime where MSD grows linearly with time. Here we define the dynamic power exponent $\alpha(t)$ to characterize the time-dependent MSD scaling for quantitative description of the crossover between these three regimes:

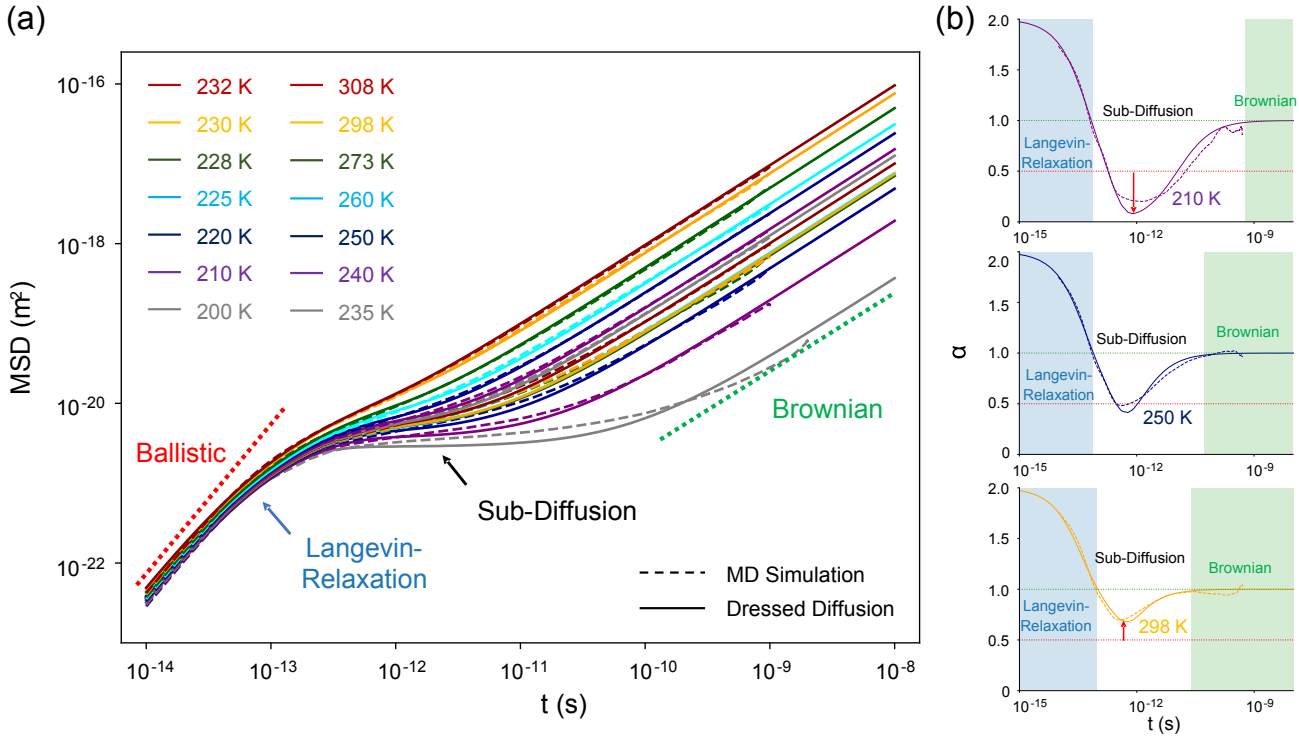

Figure 2. The diffusion dynamics in supercooled water is captured by the dressed diffusion model. (a) Time-resolved MSDs of water at temperatures from 200 K to 308 K. MSDs from MD simulation and dressed diffusion model are shown by dashed and solid lines, respectively. The red dotted line denotes the ballistic limit, and the green dotted line denotes the long-time Brownian limit. The continuous crossover from 10 to around 100 fs shows a Langevin-relaxation process, followed by the sub-diffusion regime spanning over different orders of time at various temperatures. (b) The dynamic power exponent α at 210 K, 250 K, and 298 K. The red arrows denote the deviation of minimum α from 0.5.

$$\alpha = \frac{d\log \mathrm{MSD}}{d\log t} \tag{5}$$

At tens of femtoseconds, the ballistic motion of water molecules is retrieved with the MSD proportional to the square of time, i.e., $\alpha = 2$. As time reaches 100 fs, α gradually decreases to 1, indicating the end of Langevin-relaxation regime. As time goes above the pico-second scale, the diffusive motion transforms into the sub-diffusion with $\alpha < 1$. As time further increases, the diffusion evolves into Brownian type as α approaches 1. The dynamics of α strongly depends on the temperature: when the temperature drops from 298 to 200 K, the spanned time domain of the sub-diffusion regime increases by two orders of magnitude and the minimum value of α decreases from 0.7 to 0.15, as shown in Fig. 2(b). At around 200 K, α reduces to 0.15, which is much smaller than 0.5 as predicted by the reptation polymer model[34]. Clearly, the peculiar translational dynamics of supercooled water, which was beyond the scope of previous theoretical models, is now resolved by the recent advancement of the insight from the dressed dynamics.

In addition to the characterization of the overall diffusion dynamics of supercooled water, the dressed diffusion model also unveils the detailed mechanism of the coupled relaxation processes. This is achieved by applying Eq. (3) to analyze the time dependent MSD simulated by MD with RexPoN FF to obtain values of $\langle v^2 \rangle$, a_1, a_2, b_1, and b_2 from 200 K to room temperature.

$\langle v^2 \rangle$ is the ensemble average of the instantaneous velocity of a water molecule. From 200 to 298 K, it increases from 322,000 m^2/s^2 to 501,800 m^2/s^2. This 1.56-fold increase

nicely corresponds to the 1.49-fold increase in temperature (within ±5% tolerance). This agreement reveals the equipartition principle of the kinetics in supercooled water, which establishes a linear relation between $\langle v^2 \rangle$ and the temperature T as shown in Fig. 3(a):

$$\langle v^2 \rangle = \frac{dk_B T}{m} \quad (6)$$

where d denotes the degrees of freedom for individual water molecule, m is the mass, and k_B is the Boltzmann constant. To quantify the value of d explicitly, we computed the slope,

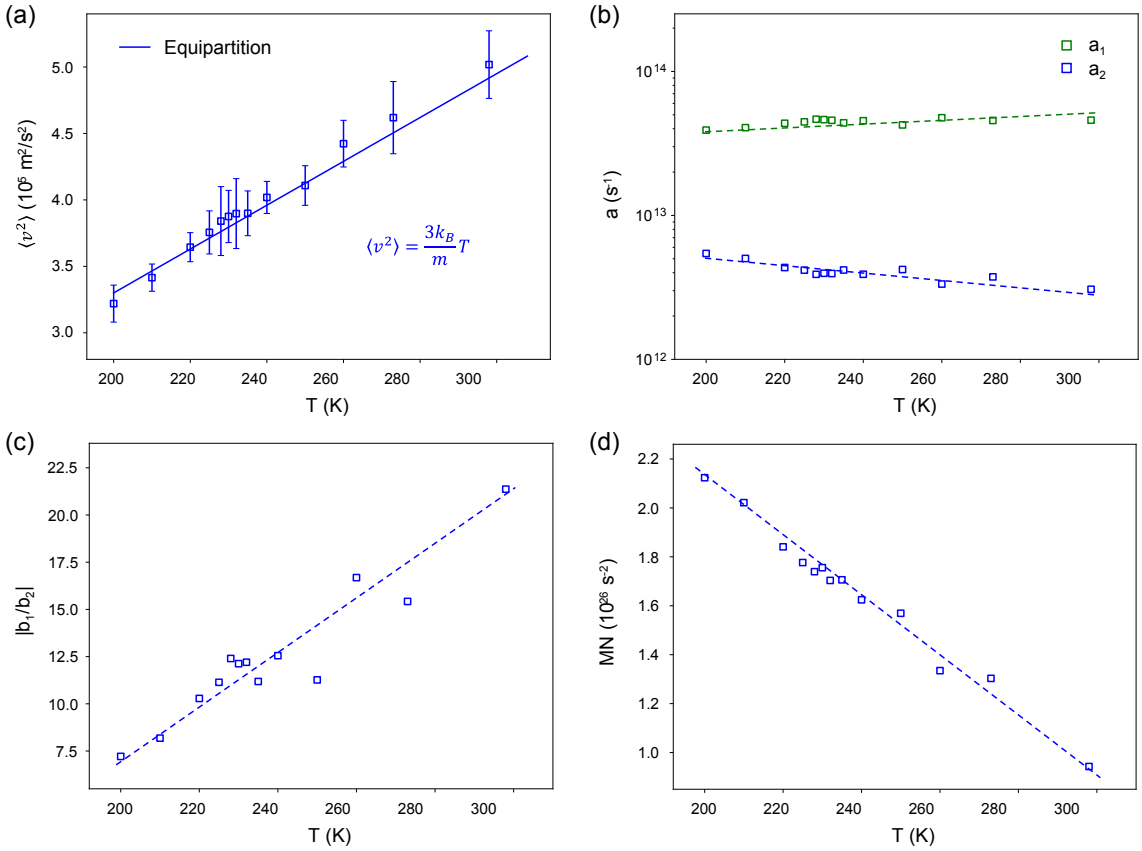

Figure 3. Two dressed relaxation modes of supercooled water extracted by dressed diffusion model. (a) The ensemble average of square instantaneous velocity $\langle v^2 \rangle$ follows the equipartition law. The solid line shows the equipartition relation fitted from the extracted $\langle v^2 \rangle$ data (blue boxes). (b) Two dressed relaxation rates a_1 and a_2 explicate the two-step relaxation at different timescales. (c) The temperature dependence of the relative intensity $|b_1/b_2|$ shows that the slow a_2-relaxation strengthens at low temperatures. (d) The coupling strength increases by around 3 folds as temperature decreases from 298 K to 200 K. The dashed lines are plotted as a guide to the eye.

i.e., $\langle v^2 \rangle / T$. The value of slope in the least-square fit analysis was 1.64×10^3 m^2·s^{-2}·K^{-1} with an overall relative standard deviation of 1.85% based on data from 200 to 298 K. Thus, the value of d is 3.15 (within ±5% uncertainty from 3.0) which reveals the individual water molecule motion in three dimensions in Langevin dynamics region.

a_1 and a_2 are the dressed relaxation rates of two separate modes. As shown in Fig. 3(b), the corresponding relaxation timescales are well separated by a one-order-of-magnitude gap. The associated intensities of two relaxation modes are measured by b_1 and b_2, which are dimensionless and have opposite signs. The relative ratio between them is depicted in Fig. 3(c). The slow relaxation mode becomes more significant at low temperatures and the fast relaxation mode dominants at high temperatures. The coupling of two different relaxations in the dressed diffusion explains the translational dynamics of water molecules in a comprehensive way, and it broadens the scope of the extended jump model that resolves the rotational relaxation of water molecules as the combination of the concerted HB jump and molecular reorientation[35,36]. Although Eq. (3) gives a simple expression for the two-step relaxation process, the complexity induced by the coupling interaction makes the underlying physico-chemical mechanism obscure, as the dressed relaxation rates a_1 and a_2 do not provide direct insight into the distinct elementary dynamics. As a result, to clarify the fundamental physics mechanism of the two different relaxations, it is essential to further analyze the decoupled self-relaxation processes at different scales

corresponding to γ_v and γ_ϕ. From the temperature-dependent analysis, we found that γ_v and γ_ϕ describe two self-relaxation dynamics with distinctive character.

- γ_v describes Langevin-type relaxation of water molecule at the timescale of fast relaxation dynamics of strong hydrogen bonds[37–39].
- γ_ϕ describes the reorganization dynamics of HB network, which might help to solve the fragile-to-strong transition of supercooled water from a dynamic perspective[14–16].

The detailed analysis and discussion of the relaxation of these two distinct physico-chemical processes will be addressed in the next sections. Here, we examine the diffusion coefficient of dressed diffusion D_{DD} at different temperatures. A quantitative agreement between the dressed diffusion coefficient and the long-time MSD evolution of MD simulation is achieved, as shown in Fig, 2(a). However, the diffusion coefficient described by the Stokes-Einstein relation, $D_{SE} = \frac{k_B T}{4\pi\eta_{SE} R}$, where η_{SE} is the classical viscosity proportional to the relaxation time of liquid structure, and R is the radius of the tracked particle, fails to explain the correct diffusion property of supercooled water. The deviation between the Stokes-Einstein relation and the supercooled water diffusion has been reported in both simulation and experiment works[10,11], and the relative difference grows several fold as the temperature decreases towards the deeply supercooled region[40,41]. The temperature-dependent decoupling of translation motion and the Stokes-Einstein viscosity is explained by the dressed diffusion coefficient D_{DD} in Eq. (4). From 298 K to 200 K, the coupling strength MN increases by around 3 folds, as shown in Fig. 3(d), which results in the temperature-dependent coupling between γ_v and γ_ϕ. At high temperatures where $MN < \gamma_v\gamma_\phi$, the γ_v-relaxation plays the dominant role. As the temperature drops, the increase of MN reflects the net effect of both enhanced HB interactions and enlarged coupling domain of the dressing field ϕ. Thus, at low temperatures where $MN > \gamma_v\gamma_\phi$, the γ_ϕ-relaxation dominates the long-time diffusion. The transition between these distinct scenarios as temperature changes manifests the breakdown of the Stokes-Einstein relation. Since this abnormal phenomenon has been reported in other liquid or soft-matter systems[42], the dressed diffusion should enlighten the broader theoretical understanding in a wide range of anomalous dynamic phenomena beyond the diffusion anomaly in supercooled water.

C. Collision-mediated Langevin Relaxation

The random collision was erstwhile among the key topics about the relaxation mechanism in particle diffusion, as it successfully explained Brownian motion and provided insight for Langevin dynamics and the fluctuation-dissipation theorem. However, it has been largely missed in the study of supercooled water, partially because of the difficulty in direct ultrafast measurement of the self-diffusion of water molecules at low temperature. In this study, the theoretical analysis based on the dressed diffusion model and MD simulation reveals the important role of this fundamental mechanism in the fast kinetic relaxation of supercooled water molecules.

The classical concept of the collision mechanism is based on the ideal model of a many-particle system at thermodynamic equilibrium. In a single-component system, every particle is modeled as a hard-sphere particle without any long-range interaction and only two-body collisions are taken into account. The velocity of the particles follows Maxwell-Boltzmann distribution, and the mean square velocity follows the equipartition law. In the thermodynamic limit, no boundary or surface effect is considered. With these assumptions, the particles always follow ballistic motions except the instants of the collision events. As a result, the collision frequency f is the inverse of the mean free time between two successive collisions: the root-mean-square velocity divided by the mean free length path:

$$f = \frac{3\sqrt{\langle v^2 \rangle}}{l} \tag{7}$$

where l is the mean free path and 3 indicates the dimension of the system. The exact expression of l depends on the specific physical condition of the system. In a dilute homogeneous system where the mean inter-particle distance is much larger than the particle diameter d, l is the inverse of the product of the particle number density n and the scattering cross section[43,44]:

$$l_1 = \frac{1}{nd^2} \tag{8a}$$

On the other hand, the inhomogeneity of microscopic liquid structure has been widely addressed and the free volume theory was developed to explain the transport properties[45–48]. From the free-volume-theory point of view, the total volume of the liquid system consists of the free volume and hard-sphere volume taken by particles, which is different from the dilute homogeneous system where the particle volume is ignored. In such a disordered hard-sphere system, the free volume expands linearly with the increase of temperature, so the mean free path follows a simple 1/3-power law with temperature:

$$l_2 = \frac{T^{\frac{1}{3}}}{\sqrt[3]{n_0 T_0}} \tag{8b}$$

where n_0 and T_0 are the reference number density and reference temperature. However, water is famous for its significant density anomaly and especially in supercooled water, the HB network preserves the long lifetime of local structural order. The mean free path in supercooled water is

thus calculated directly from the measured mass density as follows:

$$l_3 = \sqrt[3]{\frac{m}{\rho}} \tag{8c}$$

where ρ is the mass density. We use the measured mass density of water from supercooled region to above room temperature[31], then conduct polynomial extrapolation for a continuous $\rho(T)$ function substituted into Eq. (8), and get the temperature-dependent mean free path under different circumstances as shown in Fig. 4(a).

To decipher the role played by the collision mechanism addressed above, we focus on the fast relaxation step of the diffusion trajectory of supercooled water. The transient kinetics of self-diffusion in supercooled water within 100 fs is consistent with Langevin dynamics which well explains the stochastic dynamic relaxation at short times. According to Langevin equation, the scaling exponent of MSD with time decreases from 2 to 1 as the ballistic-diffusion transition caused by the decay of velocity autocorrelation, which has been discovered in ideal liquids. There are two key quantities that characterize the dynamics during Langevin process, the mean square instantaneous velocity $\langle v^2 \rangle$ and the intrinsic damping rate γ_v. As the temperature dependence of $\langle v^2 \rangle$ reveals consistence with the thermodynamic equipartition law, the temperature-dependent analysis also provides quantitative evidence for the relaxation mechanism induced by barrierless particle collision. From 200K to 298K, γ_v varies from 4.3×10^{13} to 5.0×10^{13} s^{-1}. This increase of less than 15% indicates that there is no explicit chemical activation process taking place at the related timescale. This relaxation rate is confirmed by room-temperature experiments that measured the self-diffusion coefficient of liquid water[49–51]. At room temperature, the coupling effect is relatively small, so we can neglect the coupling term and estimate the value of γ_v by Eq. (4) with the experiment data. The result shows γ_v to be around 5.2×10^{13} s^{-1}, which is only slightly higher than the value extracted from the complete MD simulation trajectories [Fig. 4(b)], because the direct measurement for the temperature-dependent coupling strength was limited by the experimental technique.

Furthermore, a direct comparison is made between the collision frequency f, derived from the classical ideal collision model, and the fast relaxation rate γ_v. We apply the equipartition relation for $\langle v^2 \rangle$, substitute l_1, l_2, and l_3 from Eq. (8) as the mean free path l under three different modelling conditions and compute the corresponding f_1, f_2, and f_3 from Eq. (7). The scaling of temperature dependence demonstrates good agreement as shown in Fig. 4(b). The value of the collision frequency f based on the collision theory are denoted by solid lines, and the extracted value of γ_v from MD simulation is marked by black box with error bars. Despite the qualitative consistence of the temperature-dependent pattern, there exists a 7-to-8 folds difference between f and γ_v. This is mainly caused by two factors:

- first, the classical collision theory applies a hard-sphere particle model, but the water molecule has a non-trivial configuration and a complex interaction including Van der Waals force and HB, which means the relaxation starts before the two water molecules ideally 'collide'.
- Second, the collision model assumes thermodynamic equilibrium without velocity correlation between water molecules. Thus f^{-1} is the timescale for the particle velocity fully loses its autocorrelation, and this process requires several rounds of basic relaxation steps, i.e., multiple times of γ_v^{-1}.

The temperature-dependent scaling indicates a systematic agreement between the classical theory of barrierless collision and the fast relation process in the diffusion dynamics of supercooled water. The scaling feature of γ_v is generally consistent with f_1 and f_3 for all temperatures, but the consistence is only valid at high temperatures for f_2. This result not only supports the general collision mechanism against detailed model settings but also enlightens the understanding of the anomalous property of the water from the nature of the fast relaxation step. For f_1 and f_3, the temperature-dependent number and mass density reflects the essence of the underlying structure order, but f_2 misses the complexity of this factor with the ideal disorder assumed. As the complexity of the water structure has been widely addressed with the two states with distinct densities, the low-density state and the high-density state, which account for the anomaly in the water density and the potential phase transition at the supercooled region. Recently, the 1D-2D transformation of the strong HB-network was found around 230 K[18]. Because of the topological transformation at 230 K, the structure order of supercooled water changes when temperature drops below 230 K, leading to failure of the f_2 model. When temperature is lower than 230 K, the water molecules in the system are linked through a connected strong HB network of 2D topological order. If the temperature is above 230 K, the strong HB network breaks into multiple disconnected clusters of disordered polymeric chains. Under such circumstances, the f_2 model stays valid. Moreover, we computed the evolution of the translational component of the kinetic entropy of water molecule (S_{tr}) at various temperatures with the two-phase thermodynamics (2PT) [52–54] method (See Supporting Information). The kinetic entropy is calculated from the vibrational density of states averaged over collections of transient trajectories with different time intervals. The entropy production process is illustrated in Fig. 4(c), which is consistent with the collision timescale of the inverse of the collision frequency. This transient process helps confirm that the underlying physics mechanism of the fast relaxation dynamics of supercooled water diffusion is due to collision-mediated relaxation as captured by classical Langevin equation.

D. Slow Relaxation Dynamics of HB Network

The long-time diffusion behavior of supercooled water has been extensively studied by both theoretical and experimental methodology. In addition to the renowned violation of the Stokes-Einstein relation that we address in the previous section, another important phenomenon is the fragile-to-strong transition at the deeply supercooled region, which can be characterized by the abrupt change of the temperature dependence of the diffusion coefficient[15]. When T is higher than the transition temperature around 230 K, the diffusion coefficient decreases as the temperature drops in a non-Arrhenius fashion, but below a temperature of 230 K it follows an Arrhenius relation that describes the strong decrease of diffusion coefficient at low temperatures, as shown in Fig. 3(d). A recent theoretical advance aimed at explaining the temperature dependence of supercooled-water diffusion, especially the fragile-to-strong transition, uses a two-state thermodynamic model where water is modeled as a mixture of two components each contributing to a distinct Arrhenius relation at separate temperature region[16]. However, the diffusion dynamics at various timescales and the underlying physico-chemical dynamics of HB network have remained elusive, which is essential to resolve the diffusion anomality of supercooled water[12].

In supercooled water, the sub-diffusion regime acts as the intermediate in the crossover from transient Langevin-relaxation to long-time Brownian motion [Fig. 2(a)]. Particularly, the power exponent α and temporal span of the sub-diffusion regime are directly associated with the long-time behavior of the diffusion coefficient, with strong temperature dependence [Fig. 2(b)]. To elucidate the dynamic mechanism of the diffusion of supercooled water, we extracted the temperature dependent slow relaxation rate γ_ϕ of the coupling field ϕ, by the dressed diffusion model. The time-dependent dressing field ϕ describes the collective interactions between single water molecule and its liquid environment made of multiple water molecules linked by the extended HB network to promote spatial correlations and cooperative motions between connected water molecules. The dynamic heterogeneity within supercooled water is thus quantified in a dynamical mean-field manner. γ_ϕ represents the reorganization dynamics of supercooled-water HB networks, which plays the key role in determining the long-time diffusion coefficient [Eq. (4)]. The γ_ϕ decreases by over 2 orders of magnitude as the temperature drops from 298 K to 200 K, while the temporal span of the sub-diffusion regime increases from a few picoseconds to around a nanosecond, accordingly. The temperature dependence of γ_ϕ does not demonstrate a unified single-Arrhenius activation behavior from 298 to 200 K, which could be explained by the topological transformation in the deep supercooled region[18]. However, we identify two distinct Arrhenius relations when separating the complete temperature domain into two regions with a transition temperature of 228 ± 3 K in the middle. These two Arrhenius laws are denoted by the different linear $\log \gamma_\phi - T^{-1}$ relations in Fig. 5(a).

Transition state theory is applied in each region to calculate the activation enthalpy and activation entropy from the temperature dependence of γ_ϕ as follows[55]:

$$\gamma_\phi = k\exp\left(-\frac{\Delta H^*}{k_B T} + \frac{\Delta S^*}{k_B}\right) \quad (9)$$

where ΔH^* is the activation enthalpy, ΔS^* is the activation entropy, k_B is the Boltzmann constant, and k is the pre-exponential factor. We conducted a linear regression to extract the slopes and the intercepts from the $\log \gamma_\phi vs\ T^{-1}$ plot in two temperature regions:

- the low-temperature region from 200 K to 225 K and
- the high-temperature region from 235 K to 298 K.

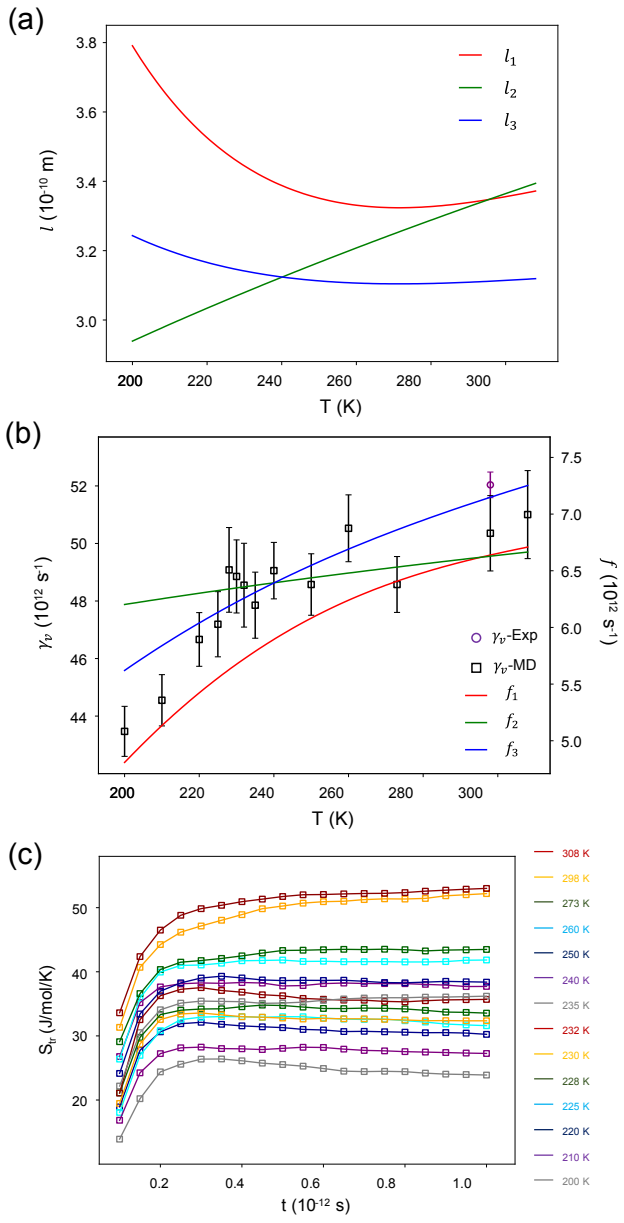

Figure 4. The characterization of Langevin-relaxation mechanism

of the barrierless collision at fast timescale. (a) The mean free path in different collision models: 1, a dilute homogeneous system; 2, a free-volume-based system; 3, a condensed system. (b) Comparison between the fast relaxation rate γ_v from dressed diffusion theory (black boxes from MD extraction and purple box from experiment with reference to the left γ_v axis) and the collision frequency, f_1, f_2, and f_3 (solid lines with reference to the right f axis), based on three collision models as in (a). (c) Production of kinetic entropy associated with translation motion of water molecule within 1 ps at different temperatures.

From 200 to 225 K, the linear regression gives a slope of -1725 K with an intercept of 18.91 with a residual of 0.00104. From 235 to 298 K, the linear regression gives a slope of -649 K with an intercept of 14.22 with a residual of 0.01456. These two linear relations are further confirmed with the relative standard deviations: the relative standard deviation is 0.152% in the low temperature region from 200 to 225 K; the relative standard deviation is 0.417% in the high temperature region from 235 to 298 K. The extrapolation of these two linear relations shows an intersection at the temperature of 229.4 K, identical to the reported transition temperature around 230 K[24,31]. A flexible transition temperature window was employed to determine the transition temperature by the intersection of the two linear extrapolations. Different temperature regions were selected and tested to confirm the transition temperature at 228±3 K. We also conducted a sensitivity analysis for the related activation enthalpy and activation entropy. (Fig. S1.)

Next, we interpret the slope and intercept for the activation enthalpy and activation entropy at each region, based on Eq. (9). In the region below 230 K, the average activation enthalpy $\Delta H_2^* = 7.86\ kcal/mol$, and in the region above 230 K, $\Delta H_1^* = 2.95\ kcal/mol$. The increase of the activation enthalpy from high to low temperatures agrees with the enhanced strong HB network due to the 1D-2D topological transition when temperature drops below 230K. Meanwhile, the two linear relations have an intercept difference as $\Delta\Delta S_{21}^* \log e/k_B + \log\left(k_2/k_1\right)$, where $\Delta\Delta S_{21}^*$ is the difference between the activation entropy of the low-temperature state and that of the high-temperature state. When the system approaches the transition temperature, the pre-factors $k_1 \approx k_2$, so the difference of the intercepts around the transition zone is contributed by the activation entropy gap during topological transition, $\Delta\Delta S_{21}^* = 10.8k_B$. This also agrees with the transformation of the topological order of strong HB network at 230 K. Because the 2D order has more HBs and enhanced network connectivity, the correlated water structure is more ordered and preserved with a lower equilibrium entropy than the 1D state. As a result, the activation entropy of 2D state is larger than 1D state, consistent with the sign of $\Delta\Delta S_{21}^*$.

As a result, in the region between 200 to 225 K, the slow relaxation dynamic process experiences an activation enthalpy of about 7.8 kcal/mol, as compared to 2.9 kcal/mol in the region between 235 to 298 K. The increment of ΔH^* in lower temperature region corroborates the increase of HB number at the presence of 2D topological connectivity. The activation enthalpy extracted by our analysis varies from 2.9 to 7.8 kcal/mol across the whole temperature domain, indicating that multiple HBs are involved in this relaxation step induced by bond-breaking and re-bonding reactions. This emphasizes the importance of the direct measurement of the reaction dynamics of HBs, since the Van de Waals interaction and local density fluctuation of water could not explain such a high activation enthalpy. Besides, the activation entropy in the lower temperature region is $10.8k_B$ higher than that in the higher temperature region. This also originates from the better ordered supercooled water with 2D strong HB network.

To investigate the thermodynamic mechanism of the discontinuous shift of ΔH^* and ΔS^* at the transition temperature, we build a three-state model as shown in Fig. 5(b). In general, the mean free energy decreases as temperature increases. In particular, the whole water system is a mixture of three molecular states, and each of them has different intrinsic enthalpy and entropy. One of the states has the highest free energy G_0 in the supercooled region from 200 to 273 K. So, it is a rare and transient state of a small fraction and a short lifetime due to its fast decay into the other states with lower free energies. This state is characterized with the highest intrinsic enthalpy H_0 and entropy S_0, indicating its potential dominance at even higher temperatures. It represents the group of water molecules that have transiently broken HBs (Trb); these are transient isolated water molecules or small molecule clusters, such as dimers or trimers, which promote the transportation dynamics. The other two states have relatively low free energies due to contributions from the connected HB networks. Due to the different orders of HB-network connectivity, one state has lower enthalpy H_2 and lower entropy S_2, making it favored in the low temperature region (200 K to 230 K), while the other has higher enthalpy H_1 and higher entropy S_1 in the high temperature region (230 K to 298 K). These two groups of water molecules associated with different strong HB network motifs are consistent with the characterization of the 1D and 2D topological orders of strong HB network from network connectivity analysis[18]. This picture provides a mixture model that sheds light on the temperature-dependent partition of water molecules in three different states. From a statistical-mechanics point of view, the relative partition between three states is determined by their intrinsic free energy: $P_i \propto \frac{1}{Z}\exp\left(-\frac{G_i}{k_BT}\right)$, where $G_i = H_i - TS_i$, denotes the free energy of each state and Z is the partition function. The partition reflects the transition dynamics between the states in the equilibrium. When

detailed balance is reached, the forward transition balances the reverse transition. As a result, the rare state has a faster transition rate toward the dominant state compared to the reverse process, clarifying the transient nature of the state with highest free energy G_0. This picture provides two different scenarios at 200-230 K and 230-298 K. From 200 K to 230 K, the 2D state has the lowest free energy and is thermodynamically favored, and from 230 K to 298 K, the 1D state starts to dominate the whole system. Based on the transition state theory, the activation barrier depends on the free energy gap between the initial and final states, i.e., $\Delta G_1 = G_0 - G_1$ at high temperature and $\Delta G_2 = G_0 - G_2$ at low temperature. As a result, two different scenarios at diverse temperature regions are clarified. When a water molecule transiently breaks its associated HBs to escape from 2D or 1D state for a long-time movement, there exist two different Arrhenius relations for this activation process, which is consistent with the distinct behaviors of γ_ϕ at the corresponding temperatures. This three-state model is further supported by the statistical analysis of the distribution of transient kinetic entropy of water molecules. The conspicuous feature in the entropy spectrum appears when applying the 2PT[52–54] method to compute entropy associated with the translational dynamic motions (See Supporting Information). As presented in Fig. 5(c), there exist three types of entropies associated with three distinct Gaussian curves. The mean value of each Gaussian curve remains unchanged throughout the whole temperature region studied in this work. When temperature changes, only the height of each Gaussian curve varies. For instance, when decreasing temperature, the intensity of the lowest entropy increases while intensities of the rest two entropy components decrease. At temperatures below 230 K, the Gaussian curve with the lowest entropy has the dominate share of the whole translational entropy in supercooled water.

From the calculated kinetic entropy of each molecule, we obtain the time-resolved entropy that characterizes the translational motion and rotation motion. We collect the translational part of the kinetic entropy for every water molecule as S_{tr} and plot the entropy spectrum in the histograms [Fig. 5(c) and Fig. S2]. We evaluate the probability density function for all temperatures from 200 to 308 K, with the kernel-density estimate based on Gaussian kernels by Scott's method[56,57]. From the continuous distribution density curve, we found there exist three distinct components with different entropies: a low-entropy component centered around 10 J/K/mol, a medium-entropy component centered around 32 J/K/mol, and a high-entropy centered around 53 J/K/mol. The intrinsic entropy as the mean value or the peak value of each component remains stable as the temperature varies. In contrast, the partition of the three components significantly changes at different temperatures: when the temperature reduces, the percentage of the component with lower entropy increases while that associated with higher entropy decreases. Based on these features, we decompose all translational entropy distributions into three distinguishable components with Gaussian distributions. Following this strategy, the three components are separated, and the relative partition associated with each state is denoted by the peak height of each Gaussian component. To further validate this three-component behavior, we conducted the calibrated Silverman's test to confirm this multi-modality of the entropy distribution[58,59] (See Supporting Information). This three-state model provides an explanation for the two-Arrhenius behavior of γ_ϕ-relaxation process at different temperature regions, with the microscopic statistics of supercooled water molecules, and helps to resolve the thermodynamic mechanism of the topological transition in the deep supercooled region.

E. Temperature Effect on HB-Network Topology

The transition-state-theory based analysis of the slow relaxation process unveils the mechanism of HB network activation. And the three-component distribution of the kinetic entropy further supports the three-state model that explains the slow relaxation dynamics with the state-dependent enthalpy and entropy. A recent study has reported that different states of water show distinct transient topological motifs with knots and links formed by entangled rings[60]. Besides, a scale-dependent persistent-homology analysis also shed light on the entangled rings in complex fluids[29]. In this section, the systematic quantification and direct characterization of strong HB network topology is made from a graph-theory point of view. We apply the graph theory method based on the Laplacian matrix to describe the topological connectivity of the strong HB network. Each node represents one water molecule. Each edge denotes the two bonded water molecules by one HB. Thus, the Laplacian matrix is constructed to quantify the HB network as follows[61],

$$L_{ij} = K_i\delta_{ij} - A_{ij} \tag{10}$$

where K_i is the number of the bonded neighbors of the node i, and A_{ij} is the adjacency matrix. The eigenvalues and eigenvectors of the Laplacian matrix are solved as λ_i and $\boldsymbol{V_i}$. The number of the zero eigenvalues reveals the disconnected components of the whole HB networks: the disconnection consistently increases when the temperature increases, i.e., high temperature facilitates the process of breaking the HB network into more separate pieces. Here, the inverse connectivity ($\tilde{C}$) as a conjugate of inverse participation ratio for individual node is employed to address the topological measure of the associated HB network of every water molecule as follows[27]:

$$\tilde{C}_j = \sum_i V_{ij}^4 \tag{11}$$

where V_{ij} is the j-th node-based component of the i-th eigenvector. This term is inspired by the inverse participation ratio that describes the localization of a certain state[25,26], whereas $\tilde{C}_j$ characterizes the j-th node's disconnectivity strength. The distribution of $\tilde{C}$ is plotted in the log-log scale as shown in Fig. 6(a). A stable region with low numerical uncertainty is selected from the peaks of the distribution curves towards $\tilde{C} = 0.3$, while most of the water molecules in the system are included. Within this region, a power-law relation is clearly identified for all different temperatures. A linear fitting is applied in the log-log distribution data to extract as a power exponent β that we define as follows:

$$P \sim \tilde{C}^{-\beta} \tag{12}$$

where P is the distribution probability of $\tilde{C}$, and β is the

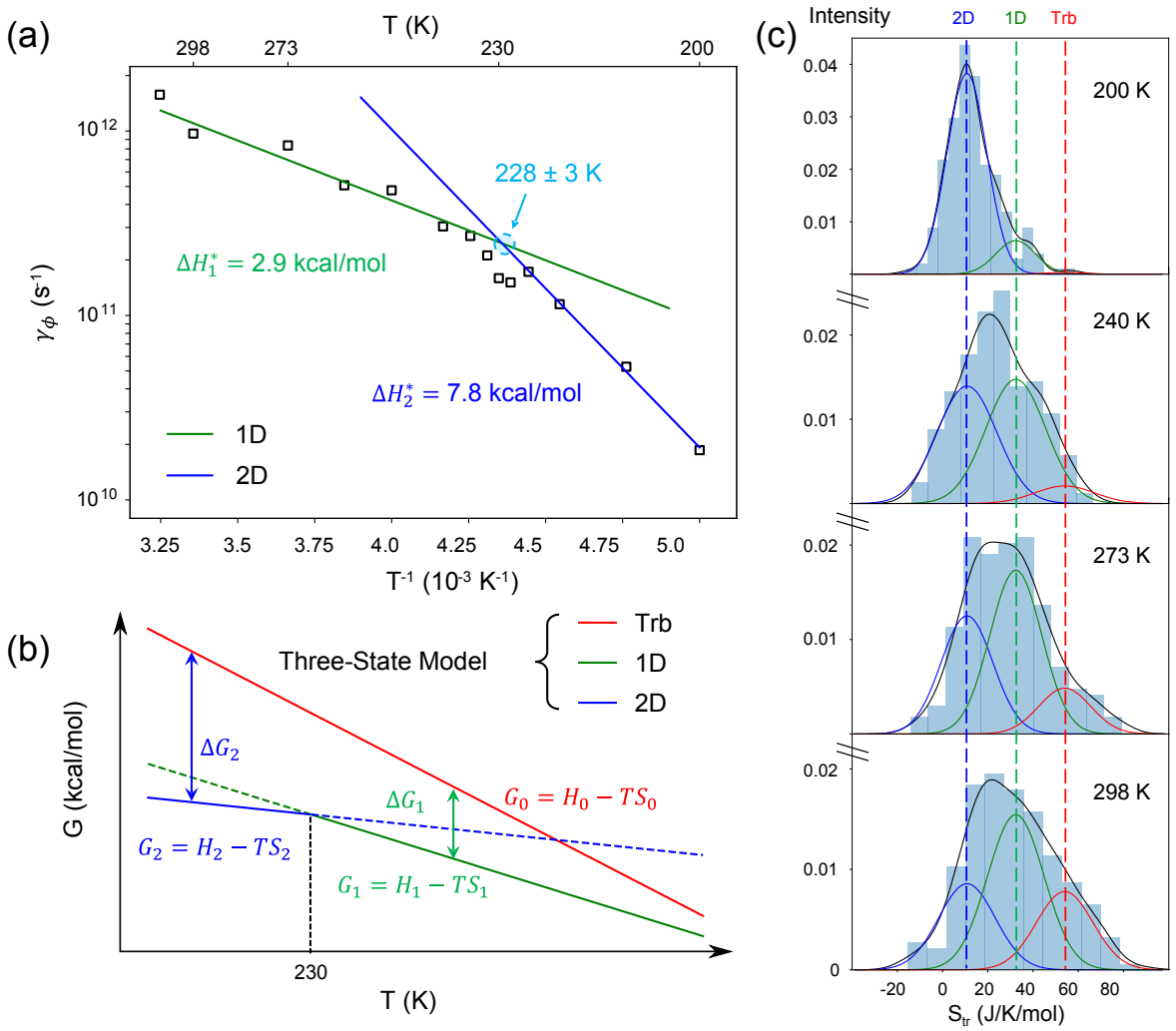

Figure 5. The temperature dependence of the slow relaxation and the three-state model explaining the underlying mechanism. (a) The temperature dependence of slow relaxation rate demonstrates the transition between two Arrhenius relations (shown by solid lines) at 228±3 K. In the low-temperature region, it shows a higher activation enthalpy and activation entropy than the high-temperature region. (b) The three-state model for this transition. The two-Arrhenius-relation activation process is explained by modeling the dressing field ϕ as a mixture of the water molecules associated with transiently broken HBs (Trb), 1D, and 2D HB networks. (c) The systematic distribution of molecular translational kinetic entropy is decomposed into three groups each with distinctive intrinsic entropy across all temperatures.

power exponent describing the characteristic scaling of the network connectivity.

Moreover, the temperature dependence of the scaling exponent β reveals the transformation of the topological order of the strong HB network from 200 K to 308 K. When the temperature is below 230 K (from 200 to 225 K), β is around 3.6, and a continuous decrease from 3.6 to 2.1 is found when the temperature increases from 232 to 308 K as shown in Fig. 6(b). The related error bar denotes the standard deviation calculated from random sampling of all strong HB network at different snapshots. The crossover of β provides a quantitative description for the temperature-dependent

topology of strong HB network. This is first revealed by the RexPoN-FF MD simulation in this work, because other empirical FFs have reported an average HB number of 4 per molecule at room temperature, which could not show the growth of HB network connectivity when temperature decreases[17]. The continuous change of β is consistent with the continuous shift of the partition of the different water components by the kinetic-entropy statistics. This implies that there is no discontinuous liquid-liquid critical point around 230 K in our simulation at 1 bar. Instead we found a transformation with a continuous temperature-dependent free energy profile[18]. These studies were generally consistent with the smooth transition reported in other simulations[22].

To directly depict the topological features of the strong HB networks, we build a rectangular lattice graph to simulate the topological order of strong HB network in supercooled water [Fig. 7(a)]. The lattice system consists of 15×15 vertices randomly connected by horizontal and vertical undirected edges. The probability of this bonding is set as 0.8 for horizontal and 0.3 for vertical connections to illustrate the 1D order, and 0.8 for both directions for the 2D order. The different probabilities along the two directions reflect the asymmetry induced by the 1D-order network topology embedded in the rectangular lattice system, and the systematic geometric symmetry could be preserved by combining it with a transposed copy of the identical topology. This setting provides a simplistic manner to mimic and visualize the strong HB network motifs. The rectangular lattice graph shares the same coordination number of 4 as water and allows the same 6-member-ring topology as the hexagon structure of water. So, it plays the role of a simplistic model to denote the topological feature of HB network. The probability parameters are set to ensure the average length of connected edges at different directions to agree with the distinct topological motifs. The probability of 0.8 corresponds to an average length of connected edges of 1.6, which means the linked HBs tend to reach over the first shell. On the other hand, the probability of 0.3 indicates that the HB within 1D network is unlikely to be formed between the neighboring pair in the vertical direction. Based on this lattice graph, the

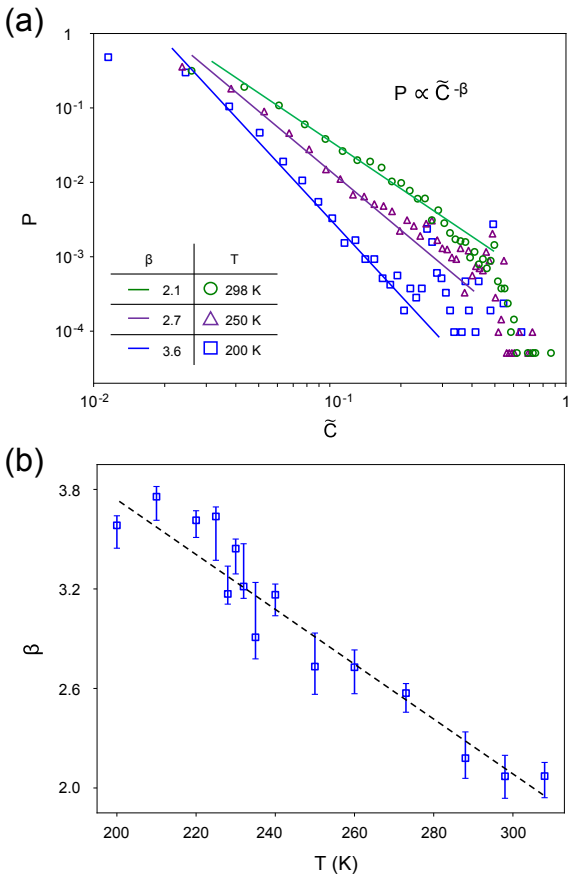

Figure 6. The graph-theory-based characterization of the strong HB-network topology. (a) The distribution of the inverse connectivity is denoted by the markers, and the power-law relations are denoted by solid lines. (b) The temperature-dependent transformation of strong HB-network topology is quantified by the measure of β.

stochastic simulation is conducted and the power exponent β is extracted from the $\tilde{C}$ distribution with 1D and 2D topologies [Fig. 7(b)]. The quantitative agreements of β values between the MD results and the rectangular lattice graph confirm the topological feature of β with visualizable insight. At low-temperature limit below 230 K, the strong HB network is dominated by the 2D topological order of β = 3.6, and the 1D order of β = 2.1 becomes obvious when T approaches room temperature. As a result, the temperature-dependent power-law scaling of $\tilde{C}$ provides a quantitative description for the topological transition of strong HB network from 1D order to 2D order when water is cooled from room temperature to the deep supercooled region below 230 K.

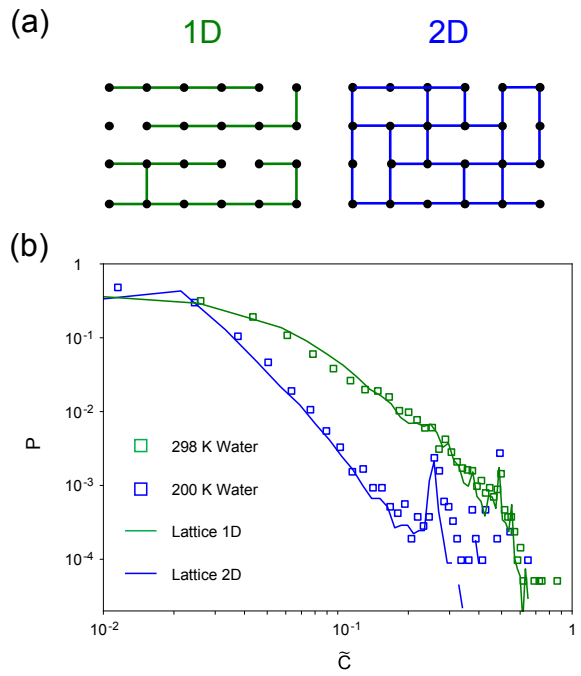

Figure 7. The topological feature of the strong HB network in water revealed by a rectangular lattice graph. (a) The schemes of two rectangular lattice graph settings for the 1D and 2D order. (b) The comparison of probability distributions of inverse connectivity between the HB network at 298 K and 200 K and the lattice graph of 1D and 2D order.

III. CONCLUSION

In conclusion, there exists a fast relaxation involving collisional relaxations that follow classical Langevin dynamics, and a slow relaxation governed by activation processes involving reorganization of the HB network. The breakdown of the Stokes-Einstein relation in supercooled water problem was resolved by dressed diffusion theory, where the abnormal diffusive motion results from dynamic coupling of multiple relaxation steps at fast and slow timescales[19]. At fast timescale, we identify the collision-mediated transient relaxation process with the relaxation time γ_v^{-1} *shorter* than the lifetime of single HB. The temperature-dependent analysis of the slow relaxation rate γ_ϕ quantitatively characterizes the activation enthalpy and entropy associated with the HB-network reorganization[1,5,16]. Moreover, a three-state model is proposed to account for the temperature modulated entropy spectrum. With the graph-theory methodology, the topological order of the strong HB network is unveiled by the power-law distribution of the inverse connectivity. Further simulation and experimental studies will provide more clues to advance our understanding of supercooled water.

CONFLICTS OF INTEREST

There are no conflicts to declare.

ACKNOWLEDGEMENTS

Support for WAG and SN was provided by the Liquid Sunlight Alliance, which is supported by the U.S. Department of Energy, Office of Science, Office of Basic Energy Sciences, Fuels from Sunlight Hub under Award Number DE-SC0021266. KCZ and HBS are supported in part by Research Grants Council of Hong Kong (16306021), HKUST grant (R9418), and Society of Interdisciplinary Research (SOIRÉE) in Hong Kong. This research made use of the computing resources of the X-GPU cluster supported by the Hong Kong Research Grants Council Collaborative Research Fund (C6021-19EF).

References

(1) Gallo, P.; Amann-Winkel, K.; Angell, C. A.; Anisimov, M. A.; Caupin, F.; Chakravarty, C.; Lascaris, E.; Loerting, T.; Panagiotopoulos, A. Z.; Russo, J.; et al. Water: A Tale of Two Liquids. *Chem. Rev.* **2016**, *116* (13), 7463–7500.

(2) Smith, R. S.; Kay, B. D. The Existence of Supercooled Liquid Water at 150 K. *Nature* **1999**, *398* (6730), 788–791.

(3) Angell, C. A. Two Phases? *Nat. Mater.* **2014**, *13* (7), 673–675.

(4) Debenedetti, P. G. Supercooled and Glassy Water. *J. Phys. Condens. Matter* **2003**, *15* (45), R1669–R1726.

(5) Anisimov, M. A.; Duška, M.; Caupin, F.; Amrhein, L. E.; Rosenbaum, A.; Sadus, R. J. Thermodynamics of Fluid Polyamorphism. *Phys. Rev. X* **2018**, *8* (1), 11004.

(6) Scala, A.; Starr, F. W.; La Nave, E.; Sciortino, F.; Stanley, H. E. Configurational Entropy and Diffusivity of Supercooled Water. *Nature* **2000**, *406* (6792), 166–169.

(7) Xu, L.; Mallamace, F.; Yan, Z.; Starr, F. W.; Buldyrev, S. V; Eugene Stanley, H. Appearance of a Fractional Stokes–Einstein Relation in Water and a Structural Interpretation of Its Onset. *Nat. Phys.* **2009**, *5* (8), 565–569.

(8) Gallo, P.; Stanley, H. E. Supercooled Water Reveals Its Secrets. *Science* **2017**, *358* (6370), 1543–1544.

(9) Gallo, P.; Sciortino, F.; Tartaglia, P.; Chen, S.-H. Slow Dynamics of Water Molecules in Supercooled States. *Phys. Rev. Lett.* **1996**, *76* (15), 2730–2733.

(10) Xia, X.; Wolynes, P. G. Diffusion and the Mesoscopic Hydrodynamics of Supercooled

Liquids. *J. Phys. Chem. B* **2001**, *105* (28), 6570–6573.
(11) Chen, S.-H.; Mallamace, F.; Mou, C.-Y.; Broccio, M.; Corsaro, C.; Faraone, A.; Liu, L. The Violation of the Stokes–Einstein Relation in Supercooled Water. *Proc. Natl. Acad. Sci.* **2006**, *103* (35), 12974–12978.
(12) Kawasaki, T.; Kim, K. Identifying Time Scales for Violation/Preservation of Stokes-Einstein Relation in Supercooled Water. *Sci. Adv.* **2017**, *3* (8), e1700399.
(13) Berthier, L.; Biroli, G. Theoretical Perspective on the Glass Transition and Amorphous Materials. *Rev. Mod. Phys.* **2011**, *83* (2), 587–645.
(14) Swenson, J.; Jansson, H.; Bergman, R. Relaxation Processes in Supercooled Confined Water and Implications for Protein Dynamics. *Phys. Rev. Lett.* **2006**, *96* (24), 247802.
(15) Xu, Y.; Petrik, N. G.; Smith, R. S.; Kay, B. D.; Kimmel, G. A. Growth Rate of Crystalline Ice and the Diffusivity of Supercooled Water from 126 to 262 K. *Proc. Natl. Acad. Sci.* **2016**, *113* (52), 14921–14925.
(16) Shi, R.; Russo, J.; Tanaka, H. Origin of the Emergent Fragile-to-Strong Transition in Supercooled Water. *Proc. Natl. Acad. Sci.* **2018**, *115* (38), 9444–9449.
(17) Naserifar, S.; Goddard, W. A. Liquid Water Is a Dynamic Polydisperse Branched Polymer. *Proc. Natl. Acad. Sci.* **2019**, *116* (6), 1998–2003.
(18) Naserifar, S.; Goddard, W. A. Anomalies in Supercooled Water at ∼230 K Arise from a 1D Polymer to 2D Network Topological Transformation. *J. Phys. Chem. Lett.* **2019**, *10* (20), 6267–6273.
(19) Zhu, K.; Su, H. Unraveling Dynamic Transitions in Time-Resolved Biomolecular Motions by A Dressed Diffusion Model. *J. Phys. Chem. A* **2020**, *124* (4), 613–617.
(20) Zhu, K.; Su, H. Generalization of Langevin Dynamics from Spatio-Temporal Dressed Dynamics Perspective. *J. Phys. Chem. A* **2020**, *124* (16), 3269–3275.
(21) Naserifar, S.; Goddard, W. A. The Quantum Mechanics-Based Polarizable Force Field for Water Simulations. *J. Chem. Phys.* **2018**, *149* (17), 174502.
(22) Hestand, N. J.; Skinner, J. L. Perspective: Crossing the Widom Line in No Man's Land: Experiments, Simulations, and the Location of the Liquid-Liquid Critical Point in Supercooled Water. *J. Chem. Phys.* **2018**, *149* (14), 140901.
(23) Palmer, J. C.; Poole, P. H.; Sciortino, F.; Debenedetti, P. G. Advances in Computational Studies of the Liquid–Liquid Transition in Water and Water-Like Models. *Chem. Rev.* **2018**, *118* (18), 9129–9151.
(24) Sellberg, J. A.; Huang, C.; McQueen, T. A.; Loh, N. D.; Laksmono, H.; Schlesinger, D.; Sierra, R. G.; Nordlund, D.; Hampton, C. Y.; Starodub, D.; et al. Ultrafast X-Ray Probing of Water Structure below the Homogeneous Ice Nucleation Temperature. *Nature* **2014**, *510* (7505), 381–384.
(25) Cavagna, A.; Giardina, I.; Parisi, G. Analytic Computation of the Instantaneous Normal Modes Spectrum in Low-Density Liquids. *Phys. Rev. Lett.* **1999**, *83* (1), 108–111.
(26) McGraw, P. N.; Menzinger, M. Laplacian Spectra as a Diagnostic Tool for Network Structure and Dynamics. *Phys. Rev. E* **2008**, *77* (3), 31102.
(27) Bakó, I.; Bencsura, Á.; Hermannson, K.; Bálint, S.; Grósz, T.; Chihaia, V.; Oláh, J. Hydrogen Bond Network Topology in Liquid Water and Methanol: A Graph Theory Approach. *Phys. Chem. Chem. Phys.* **2013**, *15* (36), 15163–15171.
(28) Otter, N.; Porter, M. A.; Tillmann, U.; Grindrod, P.; Harrington, H. A. A Roadmap for the Computation of Persistent Homology. *EPJ Data Sci.* **2017**, *6* (1), 17.
(29) Landuzzi, F.; Nakamura, T.; Michieletto, D.; Sakaue, T. Persistence Homology of Entangled Rings. *Phys. Rev. Res.* **2020**, *2* (3), 33529.
(30) He, X.; Zhu, Y.; Epstein, A.; Mo, Y. Statistical Variances of Diffusional Properties from Ab Initio Molecular Dynamics Simulations. *npj Comput. Mater.* **2018**, *4* (1), 18.
(31) Kim, K. H.; Späh, A.; Pathak, H.; Perakis, F.; Mariedahl, D.; Amann-Winkel, K.; Sellberg, J. A.; Lee, J. H.; Kim, S.; Park, J.; et al. Maxima in the Thermodynamic Response and Correlation Functions of Deeply Supercooled Water. *Science* **2017**, *358* (6370), 1589–1593.
(32) Zwanzig, R. *Nonequilibrium Statistical Mechanics*; Oxford university press, 2001.
(33) Kubo, R. Brownian Motion and Nonequilibrium Statistical Mechanics. *Science* **1986**, *233* (4761), 330–334.
(34) de Gennes, P. G. Kinetics of Diffusion-controlled Processes in Dense Polymer Systems. I. Nonentangled Regimes. *J. Chem. Phys.* **1982**, *76* (6), 3316–3321.
(35) Laage, D.; Hynes, J. T. A Molecular Jump Mechanism of Water Reorientation. *Science* **2006**, *311* (5762), 832–835.
(36) Laage, D.; Hynes, J. T. On the Molecular Mechanism of Water Reorientation. *J. Phys. Chem. B* **2008**, *112* (45), 14230–14242.
(37) Cowan, M. L.; Bruner, B. D.; Huse, N.; Dwyer, J. R.; Chugh, B.; Nibbering, E. T. J.; Elsaesser, T.; Miller, R. J. D. Ultrafast Memory Loss and Energy Redistribution in the Hydrogen Bond Network of Liquid H2O. *Nature* **2005**, *434* (7030), 199–202.
(38) Perakis, F.; De Marco, L.; Shalit, A.; Tang, F.; Kann, Z. R.; Kühne, T. D.; Torre, R.; Bonn, M.; Nagata, Y.

Vibrational Spectroscopy and Dynamics of Water. *Chem. Rev.* **2016**, *116* (13), 7590–7607.

(39) Berger, A.; Ciardi, G.; Sidler, D.; Hamm, P.; Shalit, A. Impact of Nuclear Quantum Effects on the Structural Inhomogeneity of Liquid Water. *Proc. Natl. Acad. Sci.* **2019**, *116* (7), 2458–2463.

(40) Guillaud, E.; Merabia, S.; de Ligny, D.; Joly, L. Decoupling of Viscosity and Relaxation Processes in Supercooled Water: A Molecular Dynamics Study with the TIP4P/2005f Model. *Phys. Chem. Chem. Phys.* **2017**, *19* (3), 2124–2130.

(41) Dueby, S.; Dubey, V.; Daschakraborty, S. Decoupling of Translational Diffusion from the Viscosity of Supercooled Water: Role of Translational Jump Diffusion. *J. Phys. Chem. B* **2019**, *123* (33), 7178–7189.

(42) Wei, S.; Evenson, Z.; Stolpe, M.; Lucas, P.; Angell, C. A. Breakdown of the Stokes-Einstein Relation above the Melting Temperature in a Liquid Phase-Change Material. *Sci. Adv.* **2018**, *4* (11), eaat8632.

(43) Vincenti, W. G.; Vincenti, W. C.; Kruger, C. H. *Introduction to Physical Gas Dynamics*; Wiley, 1965.

(44) Chapman, S.; Cowling, T. G.; Burnett, D.; Cercignani, C. *The Mathematical Theory of Non-Uniform Gases: An Account of the Kinetic Theory of Viscosity, Thermal Conduction and Diffusion in Gases*; Cambridge Mathematical Library; Cambridge University Press, 1990.

(45) Eyring, H.; Hirschfelder, J. The Theory of the Liquid State. *J. Phys. Chem.* **1937**, *41* (2), 249–257.

(46) Cohen, M. H.; Turnbull, D. Molecular Transport in Liquids and Glasses. *J. Chem. Phys.* **1959**, *31* (5), 1164–1169.

(47) Turnbull, D.; Cohen, M. H. On the Free-Volume Model of the Liquid-Glass Transition. *J. Chem. Phys.* **1970**, *52* (6), 3038–3041.

(48) SASTRY, S.; TRUSKETT, T. M.; DEBENEDETTI, P. G.; TORQUATO, S.; STILLINGER, F. H. Free Volume in the Hard Sphere Liquid. *Mol. Phys.* **1998**, *95* (2), 289–297.

(49) Wang, J. H. Self-Diffusion Coefficients of Water. *J. Phys. Chem.* **1965**, *69* (12), 4412.

(50) Krynicki, K.; Green, C. D.; Sawyer, D. W. Pressure and Temperature Dependence of Self-Diffusion in Water. *Faraday Discuss. Chem. Soc.* **1978**, *66* (0), 199–208.

(51) Holz, M.; Heil, S. R.; Sacco, A. Temperature-Dependent Self-Diffusion Coefficients of Water and Six Selected Molecular Liquids for Calibration in Accurate 1H NMR PFG Measurements. *Phys. Chem. Chem. Phys.* **2000**, *2* (20), 4740–4742.

(52) Lin, S.-T.; Blanco, M.; Goddard, W. A. The Two-Phase Model for Calculating Thermodynamic Properties of Liquids from Molecular Dynamics: Validation for the Phase Diagram of Lennard-Jones Fluids. *J. Chem. Phys.* **2003**, *119* (22), 11792–11805.

(53) Lin, S.-T.; Maiti, P. K.; Goddard, W. A. Two-Phase Thermodynamic Model for Efficient and Accurate Absolute Entropy of Water from Molecular Dynamics Simulations. *J. Phys. Chem. B* **2010**, *114* (24), 8191–8198.

(54) Pascal, T. A.; Schärf, D.; Jung, Y.; Kühne, T. D. On the Absolute Thermodynamics of Water from Computer Simulations: A Comparison of First-Principles Molecular Dynamics, Reactive and Empirical Force Fields. *J. Chem. Phys.* **2012**, *137* (24), 244507.

(55) Marcus, R. A. On the Theory of Oxidation-Reduction Reactions Involving Electron Transfer. I. *J. Chem. Phys.* **1956**, *24* (5), 966–978.

(56) Bashtannyk, D. M.; Hyndman, R. J. Bandwidth Selection for Kernel Conditional Density Estimation. *Comput. Stat. Data Anal.* **2001**, *36* (3), 279–298.

(57) Scott, D. W. *Multivariate Density Estimation: Theory, Practice, and Visualization*; Wiley Series in Probability and Statistics; Wiley, 2015.

(58) Silverman, B. W. Using Kernel Density Estimates to Investigate Multimodality. *J. R. Stat. Soc. Ser. B* **1981**, *43* (1), 97–99.

(59) Hall, P.; York, M. ON THE CALIBRATION OF SILVERMAN'S TEST FOR MULTIMODALITY. *Stat. Sin.* **2001**, *11* (2), 515–536.

(60) Neophytou, A.; Chakrabarti, D.; Sciortino, F. Topological Nature of the Liquid–Liquid Phase Transition in Tetrahedral Liquids. *Nat. Phys.* **2022**.

(61) Chung, F. R. K. *Spectral Graph Theory*; CBMS Regional Conference Series; Providence, RI : American Mathematical Society: Providence, RI, 1997.